Journal of Thermal Analysis and Calorimetry, Vol. 82 (2005) 171–177

ANALYSIS OF VOLUMETRIC CHANGES THROUGH MELTING USING A DILATOMETER

J. I. Frankel[1*], *W. D. Porter*[2] *and A. Sabau*[2]

[1]Mechanical and Aerospace Engineering and Engineering Science Department, University of Tennessee, Knoxville, Tennessee 37996-2210, USA
[2]Oak Ridge National Laboratory, Bethel Valley Road, P.O. Box 2008, Oak Ridge, TN 37831, USA

A conventional push-rod dilatometer is modified in order to accurately correlate the measured density to the predicted sample temperature of alloys in the phase-change regime. This new configuration makes use of a standard furnace assembly; however, the specimen is now symmetrically encased in a well-instrumented, graphite cylindrical shell. The combination of system geometry and high-conductivity sample holder material promotes the development of a simplified heat transfer model. The solution of this model properly correlates the measured density to that of the actual sample temperature based on using remote, sample-holder temperature measurements. Preliminary results using aluminum A356 provide insight into the proposed configuration.

Keywords: *heat transfer modeling, push-rod dilatometer, thermophysical properties*

Introduction

Dilatometry involves deducing volume changes as a function of sample temperature. Owing to inherent thermal lags in a system set-up, careful analysis is required to estimate the sample temperature based on remote thermocouple readings. One of the main barriers in the analysis of materials processing and industrial applications is the lack of accurate experimental data on material thermophysical properties. To date, the measurement of most high-temperature thermophysical properties is often plagued by apparent temperature lags. These temperature lags are inherent to the measurement arrangement since (a) the sample temperature cannot be directly measured and temperature data are recorded by using a thermocouple that is placed at a different location than that of the sample, and (b) there is a nonhomogeneous temperature distribution within the instrument [1, 2].

A schematic of the original Oak Ridge National Laboratory (ORNL) High Temperature Materials Laboratory (HTML) dilatometer setup for molten density measurements is shown in Figure 1a. This configuration is not geometrically optimal owing to the remote location of the single thermocouple. This configuration produces a substantial thermal lag in dynamic studies between the actual sample and thermocouple temperatures. Inferring the proper sample temperature from such a configuration requires a complicated mathematical model. Fig. 1b displays a schematic of the modified sample assembly. This 1 symmetric assembly permits lumped heat transfer models for both the sample holder and sample. Figure 2 presents photographs of the (a) old and (b) new sample configurations.

Figure 3 presents the geometric description used in the heat transfer analysis. If a temperature gradient exists between the radially placed thermocouples then an inverse heat conduction analysis [3–5] is required for estimating the surface heat flux penetrating the

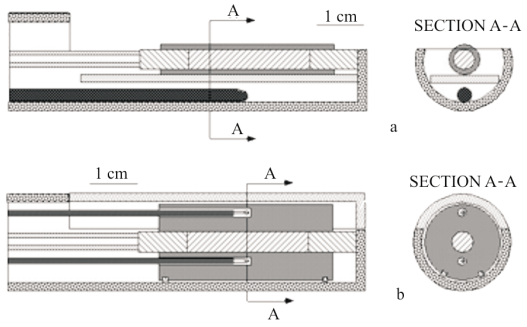

Fig. 1 Schematics showing the a – original dilatometer set up and the b – modified dilatometer

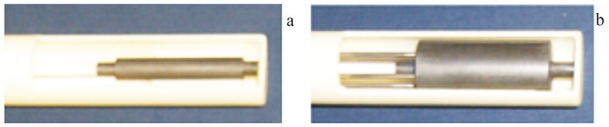

Fig. 2 Photographs showing the a – original dilatometer sample region and the b – modified dilatometer sample region with sample holder

* Author for correspondence: vfrankel@eartlink.net

1388–6150/$20.00

Akadémiai Kiadó, Budapest, Hungary
Springer, Dordrecht, The Netherlands

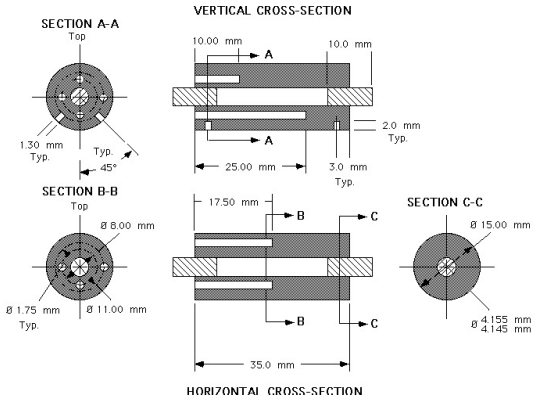

Fig. 3 Schematic of geometry showing thermocouple placements

sample. A well-designed experiment removes the need for a complicated inverse analysis. This paper (*i*) describes the sample holder modification used in the existing dilatometer, (*ii*) develops an analytic heat transfer model for the sample based on using the sample-holder temperature measurements, and (*iii*) presents preliminary numerical findings correlating the sample density to the inferred sample temperature for a common aluminum alloy in the phase-change regime.

Experimental procedure, data processing and assumptions

This section presents an overview of the entire experimental procedure used in the acquisition of the necessary data for the model developed in 'Mathematical model' 3.

Experimental procedure

The dilatometer used in the present study was a Theta Industries dual push-rod horizontal dilatometer. For the purposes of this work the dilatometer was set up in the single rod configuration. The sample holder tube and push-rod were constructed of high-purity alumina. The push-rod was attached to an LVDT (linear variable differential transformer) used for displacement measurements. The LVDT was leafspring mounted and housed in a temperature-controlled enclosure that also served as the location of the cold junction for all of the thermocouples used for specimen temperature measurements. The LVDT displacement calibration factor was determined through the use of a precision micrometer and gauge blocks. The aluminum alloy used for the study was a ternary analogue of the commercial aluminum-silicon casting alloy, A356. The composition of the ternary alloy was Al-6.92Si-0.42Mg mass% and was chosen to match the composition used in calculations of the solid fraction using DICTRA. The container developed to hold the molten specimen was a thick-walled graphite cylinder with graphite end plugs. The cylinder bore and OD of the plugs were precision ground and matched as a set to ensure a near air-tight seal while still allowing for the free movement of the end plugs required to accurately follow the changes in length of the specimen. The material used for the specimen holder and end plugs was fine-grained isotropic POCO AXF-5Q graphite whose expansion behavior had been characterized previously. The specimen holder OD was slightly less than the sample holder tube ID and was isolated from the holder tube by four small-diameter alumina pins acting as legs. The dilatometer system correction factor, which must be determined for single push-rod systems, was determined by comparing the experimentally measured values for the expansion of a NIST SRM 737 tungsten rod with the certified expansion values of the SRM. This correction run was made with the two graphite plugs from the specimen holder located on each end of the tungsten rod, as they would be during the alloy melting run, and used the same temperature schedule. The thermocouples used for the study were Type K, special grade, and were metal sheathed with closed ungrounded ends. Special precautions were taken to minimize thermally generated emfs at connections in the thermocouple circuits. The temperature schedule used for the alloy melting run was 20°C min^{-1} to 450°C followed by a 30 min isothermal hold. The heating rate then changed to 1°C min and heating was continued to a maximum setpoint of 800°C. The specimen was cooled through the solidification range at a rate of 1°C min. Data was recorded in the melting range of the alloy specimen at a rate of one reading every six seconds. Prior to testing, the dilatometer was evacuated to 100 microns using a mechanical vacuum pump and backfilled with titanium-gettered high-purity helium. This procedure was repeated three times before heating was started. A helium flowrate of 5 cm^3/s was used during the dilatometer runs.

Data processing

Processing of the dilatometer data required several steps. The raw LVDT position data (Volts) must have the system correction values, determined in the tungsten SRM run, added to it. Next the initial value of the LVDT must be subtracted from the data to result in a change in position and the LVDT calibration factor is applied to give the change in specimen length (mm). Up to the solidus temperature this delta length is used to calculate the expansion of the specimen and the specimen length and diameter at any temperature. Above the solidus temperature the graphite expansion is used to calculate the specimen container ID and specimen diameter. In this region the specimen length

is still calculated from the corrected and adjusted LVDT data. Finally the density as a function of temperature is calculated by dividing the initial specimen mass by the calculated specimen volume.

Assumptions

The calculation of density from specimen length changes determined by dilatometry requires assumptions to be made. The first assumption that must be made is that the mass of the specimen does not change during the measurement. This assumption can be validated with a check of the specimen weight after the dilatometer run and a visual inspection to assure that no molten material extruded past the end plugs. The second assumption is that the diameter of the specimen is uniform and known at all temperatures. Up to the solidius temperature of the alloy the diameter of the specimen can be calculated by applying the expansion of the alloy at a given temperature to the initial diameter. Above the solidus temperature, it must be assumed that the specimen is a fluid that takes on the shape of its container. In this region the specimen diameter is assumed to be that of the inner diameter of the graphite specimen holder, which also can be calculated from the known expansion of the graphite and the initial holder ID. This assumption is aided by the fact that the push-rod is spring loaded against the end plugs and both end plugs are free to move. During the initial region of melting of an alloy there may be a short temperature interval where the specimen has a network of solid material remaining and has not completely filled the container. The assumption of known sample diameter is not valid in this region and the density cannot be calculated for this temperature interval.

Mathematical model

ORNL has redesigned the dilatometer sample holder in order to assure the uniform heating of the test sample under consideration. This concept, used in conjunction with mathematical modeling, permits the accurate extraction of and correlation between both the sample density and predicted sample temperature. The redesigned ORNL dilatometer sample holder renders a nearly isothermal region. Four (4) embedded thermocouples, as shown in Fig. 3, are used to indicate that the container is isothermal at any instant in the experimental process. This observation is attributed to the high thermal conductivity of the shell. Additionally, the thermal mass of the sample holder is much greater than the thermal mass of the sample. Thus, only one temperature value at any instant of time is actually required. Simultaneously, the linear variable displacement transformer (LVDT) permits the length changes of the specimen to be recorded.

Preliminary analytic assumptions

Several simplifying assumptions are now related. These assumptions permit a relatively simple but robust model to be developed. Concerning the measurement, the following considerations can be made:

- The initial mass of the specimen, m, and its geometry are known at room temperature.
- Thermal expansion is accounted for in the graphite sample holder [6], end plugs, and sample.
- The sample volume follows $V(t)=V_o(1+\Delta s/s_o)^3$ in the premelt stages and is assumed to retain its cylindrical shape in the melt phase where $r_a(t)$ is the sample radius, and $\Delta s=s(t)-s_o>0$ where $s(t)$ is the sample length and so is the initial sample length at room temperature. The sample is carefully sized such that at the onset of melting; ideally speaking, the sample radius attains the value of the sample holder, i.e., $r(t)=r_a(t)$. At times this assumption is not valid (i.e., $r(t)\neq r_a(t)$ and $r_a(t)$ must be estimated therefore $V(t)=\pi r_a^2(t)s(t)$, $s(t)>s_o>0$).
- The sample length changes are obtained by adjusting the LVDT data with the corresponding thermal expansion of the graphite holder, graphite plugs and alumina rod.
- The mass of the specimen does not change with time implying $dm=0=d(\rho(t)V(t))$ where $V(t)$=sample volume. Note: $\rho(t)$ is considered known from the dilatometer but requires correlation to the sample temperature, $T_s(t)$.
- The heat capacity, $c(T_s)$, latent heat, H, and the solid fraction $f_s(T_s)$ of the sample are known.
- The output behavior of the LVDT for the push-rod dilatometer is usable for identifying the times when the sample reaches its solidus and liquidus temperatures.
- The liquidus and solidus temperatures for the sample are known.
- The furnace assembly uses Helium at 1 atm.

Melt-regime modeling

The focus of the present study lies in the melt regime of an alloy. As such, this section presents only the developments pertinent to this heat transfer regime. Let the melt regime be defined with the aid of two distinct times; namely, $t=\tau_1$ and $t=\tau_2$. Here, τ_1 is the time when the sample attains its solidus temperature ($T_s(\tau_1)=T_{sol}$, $f_s(T_s(\tau_1))=1$) while τ_2 is the time when the sample attains its liquidus temperature ($T_s(\tau_2)=T_{liq}$, $f_s(T_s(\tau_2))=0$). Key to this study is the ability to identify these times based on the LVDT output. This process

is clearly described Section 'Determinig the time domain for phase changes'. The lumped, heat equation for the sample in the phase-change regime is given by

$$-\rho(t)H\frac{\mathrm{d}f_\mathrm{s}(T_\mathrm{s})}{\mathrm{d}t}+\rho(t)c(T_\mathrm{s}(t))\frac{\mathrm{d}T_\mathrm{s}}{\mathrm{d}t}(t)= -2\frac{h(T_\mathrm{s},T)}{r_\mathrm{a}(t)}(T_\mathrm{s}(t)-T(t)),\quad \tau_1\le t\le\tau_2 \tag{1}$$

where $f_\mathrm{s}(T_\mathrm{s})\in[1, 0]$ is the solid fraction, and $h(T_\mathrm{s}, T)$ is the unknown heat transfer coefficient defined between the sample and sample holder. Note that end e.ects are neglected owing to the sample geometry. It is evident from Eq. (1) that both $T_\mathrm{s}(t)$ and $h(T_\mathrm{s}, T)$ are presently unknown. This dilemma can be resolved by introducing a physical constraint that is available from the experiment. That is, if one can identify the time at which the sample reaches the liquidus temperature then a second independent expression is generated to close the system and hence eliminate the heat transfer coefficient. The LVDT output stream possesses this information.

The solid fraction, $f_\mathrm{s}(T_\mathrm{s}(t))$ behavior is assumed known in either tabular or functional form. The solid fraction time derivative can be expressed in two components using the chain rule of differential calculus [7], namely

$$\frac{\mathrm{d}f_\mathrm{s}}{\mathrm{d}t}=\frac{\mathrm{d}f_\mathrm{s}}{\mathrm{d}T_\mathrm{s}}\frac{\mathrm{d}T_\mathrm{s}}{\mathrm{d}t} \tag{2}$$

where $\frac{\mathrm{d}f_\mathrm{s}}{\mathrm{d}T_\mathrm{s}}$ is a known property. Equation (1) can now be expressed as

$$\rho(t)\frac{\mathrm{d}T_\mathrm{s}}{\mathrm{d}t}(t)(c(T_\mathrm{s}(t))-H\frac{\mathrm{d}f_\mathrm{s}}{\mathrm{d}T_\mathrm{s}}= -2\frac{h(T_\mathrm{s},T)}{r_\mathrm{a}(t)}(T_\mathrm{s}(t)-T(t)),\quad \tau_1\le t\le\tau_2 \tag{3a}$$

subject to or $T_\mathrm{s}(\tau_1)=T_\mathrm{sol}$ or

$$\frac{\mathrm{d}T_\mathrm{s}}{\mathrm{d}t}(t)=-\frac{2h(T_\mathrm{s},T)(T_\mathrm{s}(t)-T(t))}{r_\mathrm{a}(t)\rho(t)(c(T_\mathrm{s}(t))-H\frac{\mathrm{d}f_\mathrm{s}}{\mathrm{d}T_\mathrm{s}})},\quad \tau_1\le t\le\tau_2 \tag{3b}$$

Integration of Eq. (3b) in the melt domain yields

$$T_\mathrm{s}(t)= T_\mathrm{s}(\tau_1)-2\int_{u=\tau_1}^{t}\frac{h(T_\mathrm{s},T)(T_\mathrm{s}(u)-T(u))}{r_\mathrm{a}(u)\rho(u)(c(T_\mathrm{s}(u))-H\frac{\mathrm{d}f_\mathrm{s}}{\mathrm{d}T_\mathrm{s}})}\mathrm{d}u,\quad \tau_1\le t\le\tau_2 \tag{3c}$$

where u is a dummy variable of integration. Evaluating Eq. (3c) at $t=\tau_2$ yields

$$T_\mathrm{s}(\tau_2)=T_\mathrm{liq}= T_\mathrm{sol}-2\int_{u=\tau_1}^{\tau_2}\frac{h(T_\mathrm{s},T)(T_\mathrm{s}(u)-T(u))}{r_\mathrm{a}(u)\rho(u)(c(T_\mathrm{s}(u))-H\frac{\mathrm{d}f_\mathrm{s}}{\mathrm{d}T_\mathrm{s}})}\mathrm{d}u \tag{4a}$$

where the liquidus temperature T_liq is known. Using the weighted mean-value theorem [7], the average heat transfer coefficient, $\bar{h}_\mathrm{m}$ valid in the melt domain is given as

$$\bar{h}_\mathrm{m}=\frac{T_\mathrm{sol}-T_\mathrm{liq}}{2\int_{u=\tau_1}^{\tau_2}\frac{(T_\mathrm{s}(u)-T(u))}{r_\mathrm{a}(u)\rho(u)(c(T_\mathrm{s}(u))-H\frac{\mathrm{d}f_\mathrm{s}}{\mathrm{d}T_\mathrm{s}})}\mathrm{d}u},\quad \tau_1\le t\le\tau_2 \tag{4b}$$

The reduced heat equation, defined by replacing $h(T_\mathrm{s}, T)$ by $\bar{h}_\mathrm{m}$ in Eq. (3a), becomes

$$\frac{\mathrm{d}T_\mathrm{s}}{\mathrm{d}t}(t)=-\frac{2\bar{h}_\mathrm{m}(T_\mathrm{s}(t)-(t))}{r_\mathrm{a}(t)\rho(t)(c(T_\mathrm{s}(t))-H\frac{df_\mathrm{s}}{dT_\mathrm{s}}},\quad \tau_1\le t\le\tau_2 \tag{5}$$

subject to $T_\mathrm{s}(\tau_1)=T_\mathrm{sol}$. Equation (5) has explicitly removed the need for knowing the heat transfer coefficient in lieu of introducing a physical constraint. A simple, iterative numerical procedure is implemented for determining the sample temperature $T_\mathrm{s}(t)$. Once $T_\mathrm{s}(t)$ is known then the average heat transfer coefficient, $\bar{h}_\mathrm{m}$ can be numerically determined from Eq. (4b).

For numerical convenience, the required property $\frac{\mathrm{d}f_\mathrm{s}}{\mathrm{d}T_\mathrm{s}}$ is now expressed in an analytic form based on a limited data set. It is possible to form a global approximation or interpolant for the function $f_\mathrm{s}(T_\mathrm{s})$ using the N-term truncated series [8]

$$f_\mathrm{s}(T_\mathrm{s})=\sum_{\mathrm{j}=1}^{\mathrm{N}}a_\mathrm{j}\sqrt{\beta^2+(T_\mathrm{s}(t)-T_{\mathrm{s,j}})^2} \tag{6}$$

where β is the shape factor and $\{T_\mathrm{j}\}_{\mathrm{j}=1}^{\mathrm{N}}$ represent the interpolant centers. This procedure requires the determination of the expansion coefficients $\{a_\mathrm{j}\}_{\mathrm{j}=1}^{\mathrm{N}}$ from the set of data for $f_\mathrm{s}(T_{\mathrm{s,j}})$ at measured $T_{\mathrm{s,j}}$, j=1, 2, ..., N. With this, the required property $\frac{\mathrm{d}f_\mathrm{s}}{\mathrm{d}T_\mathrm{s}}$ necessary for Eq. (2) is easily calculated by analytic differentiation.

Determining the time domain for phase changes

A typical LVDT (corrected and adjusted, see 'Experimental procedure, data processing and assumptions') sample length output over time is displayed in Fig. 4.

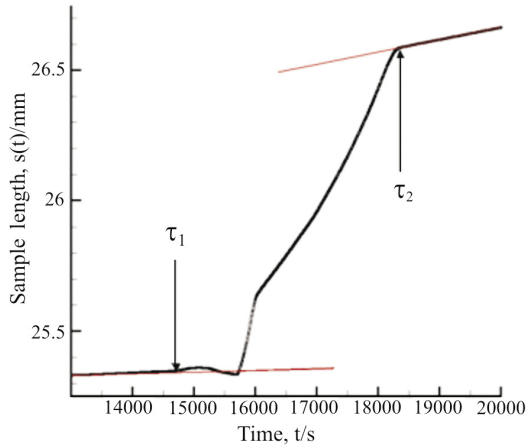

Fig. 4 Typical sample length output used to estimate τ_1 and τ_2 (programmed heating rate is 1°C min^{-1})

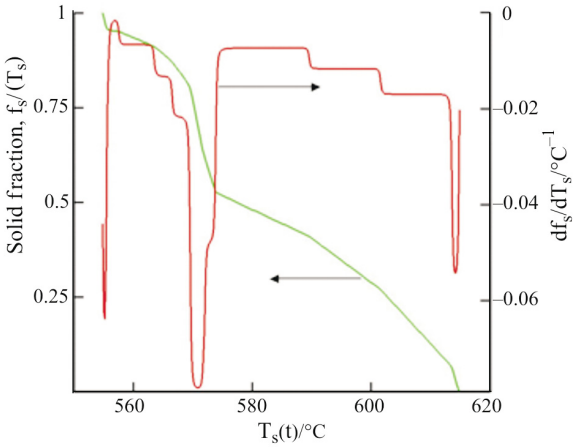

Fig. 5 Solid fraction, $f_s(T_s)$ and its sample temperature derivative, df_s/dT_s as a function of sample temperature when β^2=0.05 for A356

Data is shown prior to and past the melt regime. This output sample length plot is used to estimate τ_1 and τ_2 for the results displayed in 'Preliminary results'. The sample length output data is described by the solid circles. The solid red line segments are tangents drawn indicating a nonmelt regime. The departure points can be used to locate the values of τ_1 and τ_2. The point of detachment from the lower line segment from the data estimates τ_1 while the point of detachment from the upper line segment from the data estimates τ_2. As a physical check, the value of τ_1 should be greater than that of the time when the embedded thermocouple in the sample holder reads the value of the solidus temperature, T_{sol}. Additionally, apriori knowledge of the sample liquidus temperature should be used to physically check the value of τ_2. This time value should be greater than the time at which the sample-holder thermocouple reads the liquidus value, T_{liq}. Figure 4 data are used for the results presented in 'Preliminary results' where the heating rate is 1°C min^{-1}. in the melt domain.

Preliminary results

The focus of this research lies in developing an accurate correlation between the sample density and sample temperature for alloys in the melt regime based on remote temperature measurements. Figure 5 presents the solid-fraction data and the constructed RBF global interpolant over the sample temperature for A356. Twelve solid-fraction data points are identifiable at the locations of rapid changes in the slope. The resulting RBF approximation described in Eq. (6) uses β^2=0.05 and an equidistant distribution of centers. It is interesting to note that piecewise linear interpolation between the data points is graphically identical to the present solid line. However, numerical differentiation of piecewise continuous functions requires special care at the nodes. Additionally, it should be observed that Eq. (6) is infinitely differentiable for $\beta^2 \neq 0$. Figure 5 also presents, on the second y-axis, $\frac{df_s}{dT_s}$. For A356, an eutectic behavior is observable near 570°C and thus a large value for $\frac{df_s}{dT_s}$ is expected.

The thermophysical parameters for A356 used in this preliminary investigation are taken as H=429J g^{-1} [9], $c(T_s)$=c=1.19 kJ/(kg K) [9] while the sample mass is measured as 0.87709 g. The initial geometric length of the specimen, so is 25.001 mm while the sample diameter and inner diameter of the holder are 4.107 mm and 4.145 mm, respectively. The solidus and liquidus temperatures are 551 and 614°C, respectively. The total number of temporal data points used in the region defined by τ_1=14650 sec and τ_2=18359 sec is 582 points. It is presently assumed that $r_a(t)$=$r(t)$. The preliminary test case uses a heating rate of 1°C min^{-1} from t≈8000 sec to t≈28000 sec. The sample was maintained at an isothermal hold prior to experiencing this heating rate in order to assure system equilibrium. With the collected sample-holder temperature data, the numerical procedure is implemented for estimating the sample temperature based on Eq. (5). The iterative numerical procedure required 23 iterations using a conventional, forward Euler method with a relaxation constant of 0.5. Trapezoidal rule integration is used for calculating $\bar{h}_m$. It is determined that $\bar{h}_m$=1.99 kW/(m^2 °C). This value for the average heat transfer coefficient lies within the estimated bandwidth given in [10] (p. 90, Fig. 5.13 at the onset of the experiment which corresponds to a similar physical problem and material as proposed here).

Figure 6 presents the sample length, $s(t)$ and thermocouple temperature data, $T(t)$ in the melt domain time

span given by $t \in [\tau_1, \tau_2]$. The LVDT voltage has been carefully converted to displacement in this figure. Figure 7 presents the density, $\rho(T_s)$ as a function of the numerically calculated sample temperature using the proposed numerical procedure. This figure also presents the solid fraction in order for the reader to clarify the density behavior in the vicinity of the eutectic temperature (570°C). Finally, Fig. 8 presents the sample holder temperature, $T(t)$ and sample temperature, $T_s(t)$ over the melt time domain. The eutectic behavior of a material a.ects the sample temperature upon external heating. The embedded thermocouple temperature readings continue to rise as energy is continuously deposited into the system from the heater. However, the sample temperature, upon encountering an eutectic region, tends to remain relatively flat (see Eq. 5 as $df_s/dT_s \to \infty$). For this example, the analysis adjusts the sample temperature by approximately 0.75°C as indicated by the second y-axis detailing the temperature difference between the sample and the holder, $T(t)–T_s(t)$ over the time span of interest.

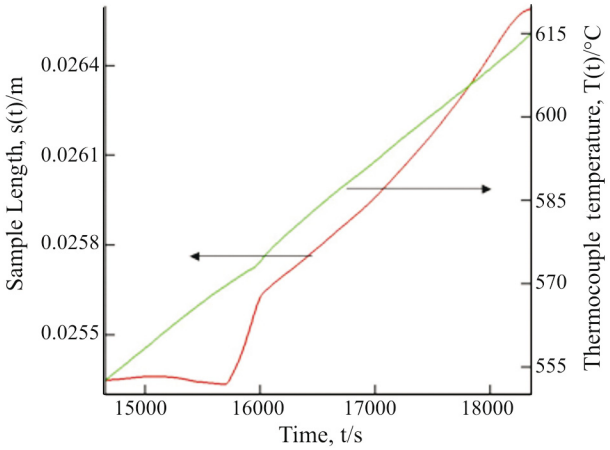

Fig. 6 Sample length, $s(t)$ and thermocouple temperature, $T(t)$ *vs*. measured time t in melt regime

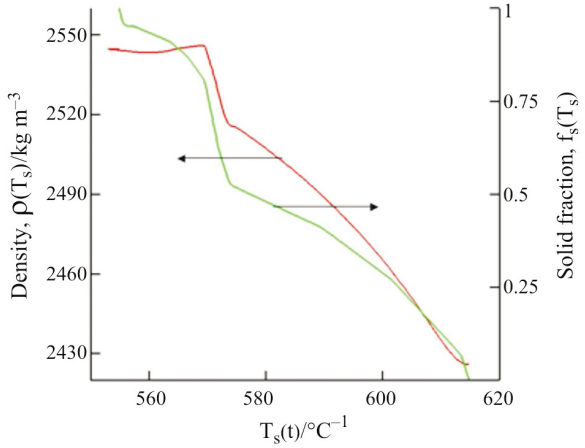

Fig. 7 Desired density, $\rho(T_s(t))$ and solid fraction, $f_s(T_s(t))$ as a function of predicted sample temperature, $T_s(t)$

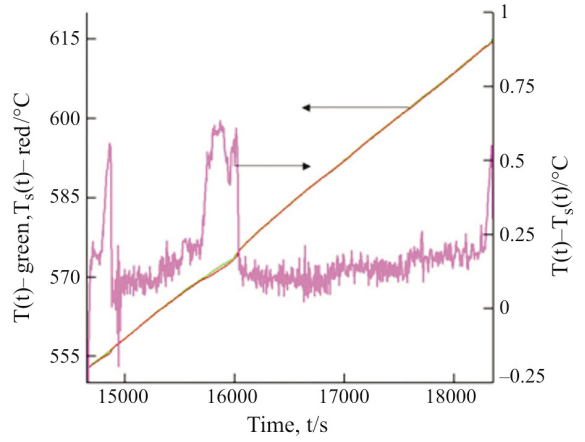

Fig. 8 Comparison between thermocouple temperature, $T(t)$ and predicted sample temperature, $T_s(t)$ over time t

Conclusions

This preliminary experimental investigation reveals that it is possible to accurately infer the sample temperature based on sample-holder temperature measurements using the proposed modified holder assembly. This inference is obtained through the careful orchestration of experimental design and analysis. This configuration minimizes geometrically induced lags and accounts for the phase-change induced lag, through a mathematical model, as measured from a distant thermocouple in the sample holder. The results presented here offer insight into developing a dilatometer holder assembly that permits the characterization of high-temperature alloys in the melt regime. Sample density measurements are now correlated with an estimated sample temperature that accounts for thermal lags inherent to the dilatometer design. Further refinements could involve (*i*) experimentally determining the sample latent heat, H and specific heat, c_p, and (*ii*) refining the solid fraction curve to include additional data points and thereby obtain a smoother representation of its derivative with respect to temperature.

Acknowledgements

This work was supported under a DOE grant provided to the University of Tennessee under the Industrial Materials for the Future Program (DE-FC-7-01ID14249)

References

1 Metalcasting Industry Technology Roadmap, Metal Coalition of the American Foundrymen's Society, Jan. 1998.
2 Steel Industry Technology Roadmap, Steel Industry, March 1998.

3 J. V. Beck, B. Blackwell and C. R. St. Clair, Inverse Heat Conduction, Wiley and Sons, New York 1985.
4 K. Kurpisz and A. J. Nowak, Inverse Thermal Problems, Computational Mechanics, United Kingdom 1995.
5 D. M. Trujillo and H. R. Busby, Practical Inverse Analysis in Engineering, CRC Press, Boca Raton FL, 1997.
6 J. G. Hust, NBS Special Publications 260–89, Washington DC, 1984.
7 W. Kaplan, Advanced Calculus, Addison-Wesley, Reading MA, 1973.
8 R. L. Hardy, Computers Math. Appl., 19 (1990) 163.
9 Auburn University Materials Processing Center Materials Database (http://metalcasting.auburn.edu/data/).
10 D. M. Stefanescu, Science and Engineering of Casting Solidification, Kluwer, New York 2002.

Received: January 15, 2004
In revised form: June 14, 2005

DOI: 10.1007/s10973-005-6813-6

DOI: 10.1007/s10973-005-3004-4